CNT-based MEMS/NEMS gas ionizers for portable mass spectrometry applications

Citation: Velasquez-Garcia, Luis Fernando, Blaise Laurent Patrick Gassend, and Akintunde Ibitayo Akinwande. "CNT-Based MEMS/NEMS Gas Ionizers for Portable Mass Spectrometry Applications." Journal of Microelectromechanical Systems 19.3 (2010): 484–493. Web. 25 May 2012. © 2010 Institute of Electrical and Electronics Engineers

As Published: http://dx.doi.org/10.1109/JMEMS.2010.2045639

Publisher: Institute of Electrical and Electronics Engineers (IEEE)

Persistent URL: http://hdl.handle.net/1721.1/70945

Version: Final published version: final published article, as it appeared in a journal, conference proceedings, or other formally published context

CNT-Based MEMS/NEMS Gas Ionizers for Portable Mass Spectrometry Applications

Luis Fernando Velásquez-García, *Member, IEEE*, Blaise Laurent Patrick Gassend, and Akintunde Ibitayo Akinwande, *Fellow, IEEE*

***Abstract*—We report the fabrication and experimental characterization of a carbon nanotube (CNT)-based MEMS/NEMS electron impact gas ionizer with an integrated extractor gate for portable mass spectrometry. The ionizer achieves low-voltage ionization using sparse forests of plasma-enhanced chemical-vapor-deposited CNTs as field emitters and a proximal extractor grid with apertures aligned to the CNT forests to facilitate electron transmission. The extractor gate is integrated to the ionizer using a high-voltage MEMS packaging technology based on Si springs defined by deep reactive ion etching. The ionizer also includes a high-aspect-ratio silicon structure (μfoam) that facilitates sparse CNT growth and also enables uniform current emission. The devices were tested as field emitters in high vacuum (10^{-8} torr) and as electron impact ionizers using argon at pressures of up to 21 mtorr. The experimental data show that the MEMS extractor gate transmits up to 66% of the emitted current and that the ionizers are able to produce up to 0.139 mA of ion current with up to 19% ionization efficiency while consuming 0.39 W. [2009-0246]**

***Index Terms*—Carbon nanotubes (CNTs), deep reactive ion etching (DRIE), electron impact ionization, field emission, gas ionizer, portable mass spectrometry (MS), 3-D MEMS packaging.**

I. Introduction

MASS SPECTROMETERS are powerful analytical tools that are helpful to quantitatively determine the chemical composition of a sample. Unfortunately, conventional mass spectrometry (MS) hardware is bulky and power hungry, which limits the range of applications that the technology can satisfy. The development of gas chromatography and MS (GC/MS) systems that are small, light, mechanically and thermally robust, and low-powered would enable their portability and therefore would expand the applicability of MS techniques. Portable GC/MS systems, either as individual units or as part of massive networks, can be used in a wide range of *in situ* applications including geological survey, law enforcement, environmental monitoring, process monitoring, and space exploration [1]–[12].

The four major components of an MS system are the ionizer, the mass filter, the detector, and the pump. The ionizer transforms the molecules of the sample to be analyzed into charged fragments, the mass filter sorts these ions according to their mass-to-charge ratios, the detector counts the number of ions that are transmitted by the mass filter, and the pump keeps the system at a pressure level that allows all the other subsystems to operate with good reliability [13]. The power consumption, size, and weight of an MS system are driven by the pumping requirements. Therefore, relaxation of the vacuum level at which the system components can operate is needed to enable its portability [14], [15].

There is a substantial number of reports in the literature on miniaturized MS components using conventional machining technologies, including fully functional MS systems [16], [17]. Even though these instruments achieve good performance, the machining methods involved in their making are relatively expensive, hence limiting the applicability of the technology. The use of micro- and nanofabrication technologies to implement miniaturized MS hardware would enable batch fabrication and would further reduce the dimensions of the components, which could lead to MS components with better performance. In addition, microfabricated technologies have the potential of implementing systems with higher performance through better component integration [18].

MEMS-based analytical instrumentation has been an active area of research for over three decades [19]. The literature on MEMS MS components concentrates on the development of scaled-down mass filtering hardware including time of flight [20], ion trap [21], ion mobility [22], and quadrupole mass filters [23]–[27]. There are also reports of MEMS detectors [28], [29] and MEMS vacuum pumps for portable applications [30]–[32]. The majority of the work reported on MEMS/NEMS ionizers is based on electron impact ionization. In an electron impact ionizer (EII), a stream of electrons is used to ionize neutral gas molecules by collision. Yoon *et al.* reported a MEMS ionizer that uses a tungsten filament [33], a nickel filament [34], or carbon nanotubes (CNTs) [34] as electron source, although no ionization data were provided. Other researchers have developed CNT-based EIIs suitable for portable MS, including Hwang *et al.* [35], Bower *et al.* [36], Chen *et al.* [37], Park *et al.* [38], and Manohara *et al.* [39]. In addition, low-power, portable, and high-pressure operation compatible glow-discharge ionizers have been developed. For example, Gao *et al.* reported spectra from a miniaturized glow discharge

Manuscript received October 9, 2009; revised January 25, 2010; accepted March 9, 2010. Date of publication April 19, 2010; date of current version June 3, 2010. Subject Editor R. R. A. Syms.

L. F. Velásquez-García is with the Microsystems Technology Laboratories, Massachusetts Institute of Technology, Cambridge, MA 02139 USA (e-mail: lfvelasq@mit.edu; pegasus@mtl.mit.edu).

B. L. P. Gassend was with the Department of Electrical Engineering and Computer Science, Massachusetts Institute of Technology, Cambridge, MA 02139 USA. He is now with Willow Garage, Inc., Menlo Park, CA 94025 USA (e-mail: gassend@alum.mit.edu; blaise.gassend_jmems@m4x.org).

A. I. Akinwande is with the Department of Electrical Engineering and Computer Science, Massachusetts Institute of Technology, Cambridge, MA 02139 USA (e-mail: akinwand@mtl.mit.edu).

Color versions of one or more of the figures in this paper are available online at http://ieeexplore.ieee.org.

Digital Object Identifier 10.1109/JMEMS.2010.2045639

ionizer that is able to operate at 10^{-2}-torr-level pressures [40], and Longwitz *et al.* reported a MEMS glow-discharge ionizer intended for ion mobility MS [41]. However, these devices have reliability problems due to sputtering of the electrodes caused by the arc [42].

In an EII, the ratio between the ion current $I_I(E)$ and the electron current $I_E(E)$ is [43]

$$\frac{I_I(E)}{I_E(E)} = \frac{P}{K_b \cdot T} \cdot L \cdot \sigma_{\text{total}}(E) \tag{1}$$

where E is the energy of the electrons, P is the gas pressure, K_b is the Boltzmann's constant, T is the gas temperature, L is the ionization collision path length (i.e., the distance between the electron source and the ion collector), and σ_{total} is the total ionization cross section along the ionization collision path length. State-of-the-art EIIs for MS systems accomplish ionization using a thermionic electron source. Thermionic cathodes require high temperature (> 2000 K) to operate [44], which results in inefficient power consumption (typical thermionic ionizers consume 5 W), as well as in reliability issues if they are operated at high pressure ($> 10^{-4}$ torr) due to the chemical reactivity of the cathode surface, particularly if the gas mix contains oxygen [13], [45]. Therefore, thermionic-based EIIs are not ideal for portable MS.

A low-power approach to implement EIIs for portable MS systems involves the use a cold cathode. Electrons are field emitted from the surface of metals and semiconductors when the potential barrier that holds electrons within the material (workfunction ϕ) is deformed by the application of a high electrostatic field [46]. High surface electrostatic fields are typically obtained by the application of a voltage to a high-aspect-ratio structure with nanometer-scaled tip radius. Field emission is described by the Fowler–Nordheim (FN) equation, which states that the electron current $I_E(V_G)$ emitted from a tip biased at a voltage V_G with respect to the gate has a strong dependence on the field factor β of the tip

$$I_E(V_G) \propto \beta^2 \cdot V_G^2 \cdot \exp\left[-\frac{B \cdot \phi^{1.5}}{\beta \cdot V_G}\right]. \tag{2}$$

In (2), B is equal to 6.8×10^7 when V_G and ϕ are in volts and the field factor is in per centimeter [46]. The field factor β relates the electric field at the surface of the tip to the applied gate voltage, and it is, to first order, equal to the inverse of the emitter tip radius r [47]. Field-emission cathodes have a faster response than thermionic cathodes because the time lag in a thermionic source is controlled by its thermal inertia, while the time lag in a cold cathode is set by the RC time constant involved in charging the electrodes.

The reliability of cold cathodes operated at high pressure is affected by back-ion bombardment and by chemical degradation. In the first case, back-streaming ions could impact and blunt the sharp tips, hence reducing their field factor. However, the addition of a second proximal gate to the basic field emitter diode configuration [48] could visibly mitigate back-ion bombardment if the second gate is biased at a more negative voltage than the bias voltage of the field emitter, effectively acting as collector of the back-streaming ions. In the second case, the gas mix can contain reactive gases such as oxygen that could degrade the performance of the field emitters by increasing the workfunction of the emitting surface or by increasing the emitter tip radii due to the formation of a film on top of the emitter. In particular, chemical degradation due to oxygen strongly affects the performance of metallic field emitters, even for very low oxygen partial pressures [49].

Cold cathodes that use CNTs as field emitters are an attractive option in implementing EIIs for portable MS, because CNTs have large field factors due to their nanoscaled diameters and very high aspect ratios [50]. In addition, the remarkable physical properties and good chemical resistance of CNTs [50] address the back-ion bombardment-related and oxygen-related reliability issues of the EIIs. For example, Gadaska *et al.* reported single-gated CNT-based cathodes with long-term reliability while operating in an oxygen atmosphere at 10^{-4}-torr-level pressures [51]. Also, Chen *et al.* reported the operation of EIIs at mid millitorr-level pressures with no noticeable degradation using an array of double-gated CNTs as cathode [37]. In this paper, we report the operation of a CNT-based EII at 10^{-2}-torr-level pressure with no noticeable performance degradation and without using a second gate.

This paper is based on previously reported work from our group that explored sparse growth of CNTs without lithography for gas ionizers [52], [53]. This paper focuses on producing ions through electron impact ionization while providing a more comprehensive description of the technology. We also present new data that demonstrate more than two orders of magnitude larger ion current and almost a fourfold increase in the ionization efficiency than previously reported. Section II of this paper describes the structure and design of the CNT-based EII. Section III provides a description of the fabrication of the devices, and it also provides characterization of the fabrication using SEMs. Section IV presents and analyzes the data from the devices as electron field emitters and EIIs, and it compares the results with the literature.

II. Device Structure and Design

The MEMS/NEMS CNT EII is composed of two substrates, i.e., a main body and an extractor gate, as shown in Fig. 1. Fig. 2 shows a set of SEMs that illustrate the structure of the main body substrate. The main body is a two-wafer stack that includes sparse arrays of plasma-enhanced chemical vapor deposited (PECVD) CNTs, a high-aspect-ratio silicon structure (μfoam), and a system of deep reactive ion etched (DRIE) springs to assemble the extractor to the main body. The extractor is a 1-cm-wide disk-shaped component with a perforated grid at its center, which includes a set of eight notches at its boundary. The notches are used to lock in the extractor substrate to the main body substrate, as shown in Fig. 3. The μfoam and the extractor grid do not line up, as shown in Fig. 4, because the extractor is used as a shadow mask during the deposition of the CNT catalyst (see Section III).

The MEMS/NEMS CNT EII includes a set of features to achieve low-voltage ionization, high-pressure operation, and device reliability. First, the device uses sparse forests of PECVD CNTs as field enhancers. The clusters of CNTs are

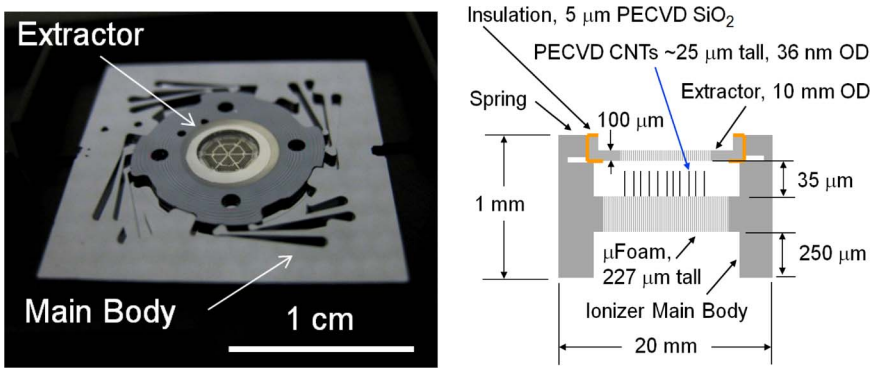

Fig. 1. (Left) Field view and (right) cross-sectional schematic of the MEMS/NEMS CNT EII. The ionizer is composed of an extractor gate and a main body that includes a high-aspect-ratio silicon structure, sparse PECVD CNT forests as field enhancers, and a set of DRIE-patterned springs for assembly of the extractor gate. The boundary of the extractor has a 5-μm-thick PECVD silicon dioxide coating that provides electrical insulation between the extractor and the rest of the device. The vertical separation between the CNT tips and the extractor is about 10 μm. The boundary of the CNT forest is a 2-mm-diameter circle.

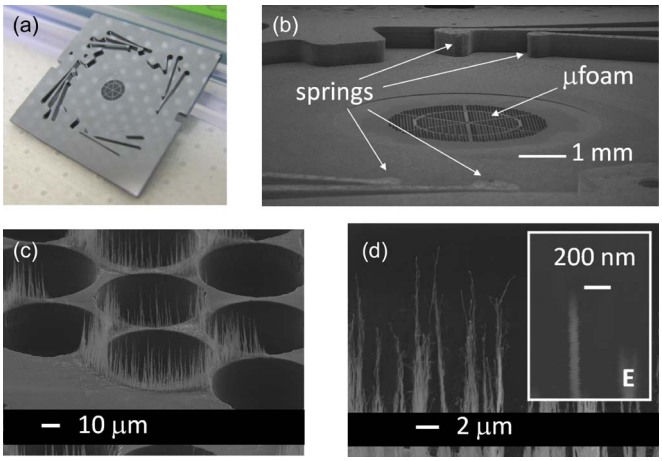

Fig. 2. (a) Field view photograph of the ionizer main body, (b) field view SEM of the central part of the main body showing the μfoam and the DRIE-patterned spring assembly system, (c) field view SEM of a sparse PECVD CNT forest on top of the μfoam, (d) close-up SEM of the PECVD CNTs, and (e) close-up SEM of a CNT tip. The typical CNT tip radius is about 36 nm.

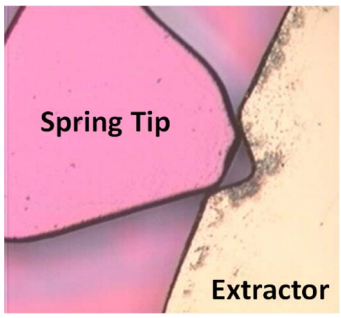

Fig. 3. DRIE spring tip of the ionizer main body substrate locked into a notch on the boundary of the extractor substrate. The main body substrate has eight springs that are evenly distributed across the boundary of the extractor to assemble the extractor substrate to the rest of the ionizer.

sparse to diminish the shadowing effects due to the proximity between field enhancers. CNTs are resilient high-aspect-ratio graphitic structures with nanoscaled tip diameters ideal for field-emission applications [54], and they can operate as electron sources at high pressure ($> 10^{-4}$ torr). We had previously shown that it is possible to grow sparse clusters of PECVD CNTs without high-cost/low-throughput methods, such as e-beam lithography, by depositing the CNT catalyst (Ni) on

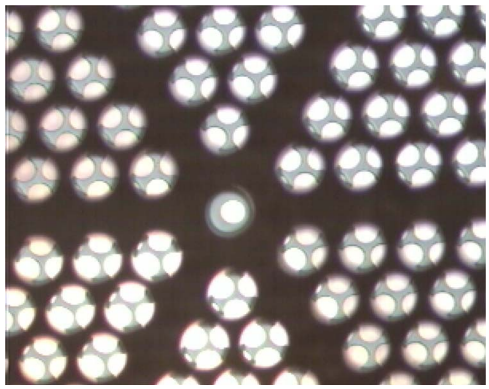

Fig. 4. Backlight top view of the extractor grid on top of the μfoam.

top of the μfoam [52]. Second, the device uses a MEMS proximal extractor gate that is held a few micrometers above the PECVD CNT tips. The proximal gate enables electron emission at low voltage. The extractor gate is integrated to the rest of the ionizer using a high-voltage MEMS packaging technology based on DRIE-patterned mesoscaled deflection springs [55]. We have shown that this packaging technology is capable of reversibly assembling mesoscaled parts with as little as 6.2 μm of biaxial misalignment and 0.6 μm of assembly repeatability, and it can also withstand large inertial forces without detaching [56]. This assembly approach makes it possible to use the extractor as a shadow mask to define the catalyst pads, then, to grow the PECVD CNTs without the extractor gate assembled, and, finally, to re-assemble the extractor to obtain a functional device. A distinct advantage of this approach is that it prevents plasma-induced damage of the silicon dioxide film on the surface of the extractor during CNT growth. The high degree of re-assembly alignment precision between the extractor and the CNT growth is reflected in the large electron current transmission through the extractor, which is almost two orders of magnitude larger than the electron current transmission of a nonaligned extractor using a similar emitting substrate and testing rig (see Section IV) [52]. Third, we previously showed that it is possible to achieve current limitation in the electron current if the device is made of a lowly doped silicon ($\sim 10^{13}$ cm^{-3} doping concentration) [53]. The current limitation is presumably due to the high aspect

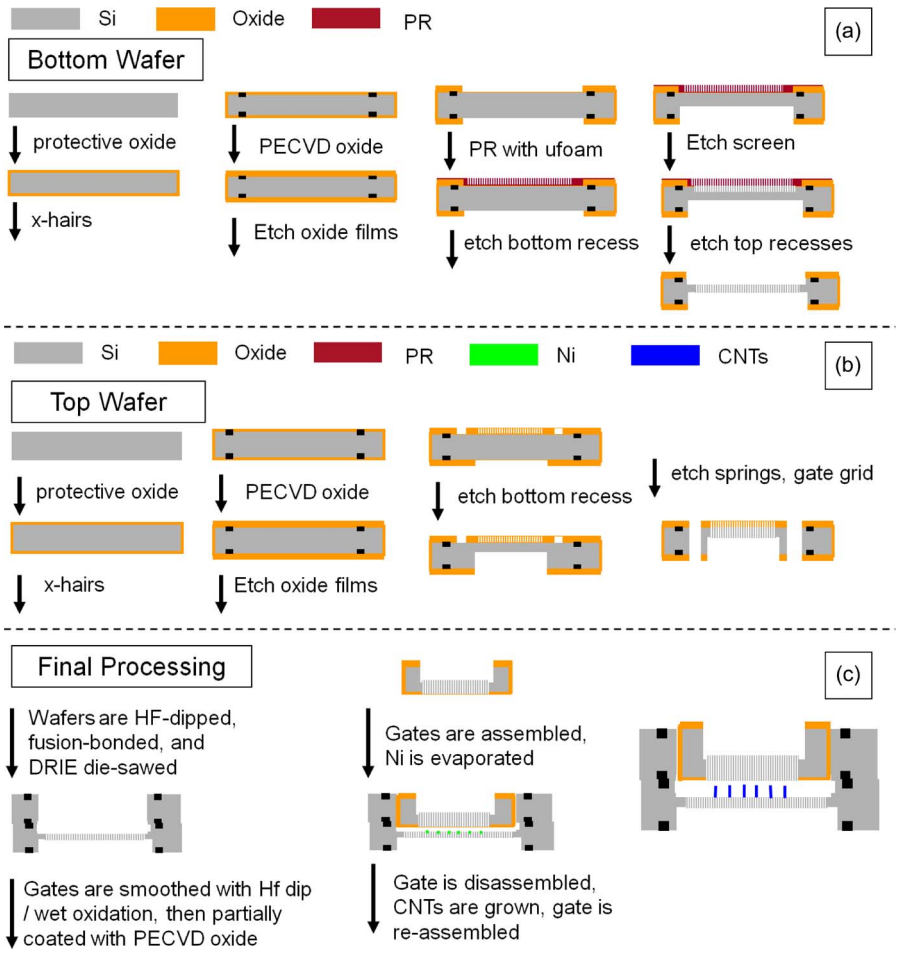

Fig. 5. Process flow to fabricate the MEMS/NEMS CNT EIIs: fabrication process flow of the (a) bottom wafer, (b) top wafer, and (c) final processing.

ratio of the μfoam, pinch off of the conduction channel due to the applied voltage, and the velocity saturation at high fields of electrons within the semiconductor lattice, resulting in more spatially uniform current emission [57], [58]. Finally, the design of the ionizer can potentially simplify the overall MS system integration by including a structure (i.e., the μfoam) that can serve as an interface between the interior and exterior of the MS. The μfoam acts as a perforated screen that feeds the exterior atmosphere into the MS at a rate controlled by the viscosity and the compressibility of the gas [59].

III. Fabrication

The MEMS/NEMS EIIs are fabricated using two 6-in silicon wafers that are 500 μm thick. The two wafer substrates are used to fabricate the main body of the ionizers, while portions of one of the wafers are used to fabricate the extractor gates. The process flow in fabricating the bottom wafer is shown in Fig. 5(a), the process flow in fabricating the top wafer is shown in Fig. 5(b), and the final joint process flow is shown in Fig. 5(c). The initial fabrication steps of both wafers are identical. First, a 0.3-μm-thick thermal silicon dioxide film is grown on the wafers to protect their bonding surfaces from damage during processing. Then, alignment marks are etched on both sides of the wafers using contact lithography on a 1-μm-thick spin-coated photoresist (PR) and reactive ion etching (RIE) of the exposed silicon dioxide film and the silicon substrate directly underneath. Next, the PR is stripped off, and both sides of the wafers are coated with a 4-μm-thick PECVD silicon dioxide film that is annealed at 950 °C in nitrogen. The silicon dioxide films are used as hard masks in later etch steps. After the PECVD silicon dioxide films are annealed, the process flow continues as follows.

A. Bottom Wafer Process Flow

The silicon dioxide films on both sides of the wafer are etched using contact photolithography on 10-μm-thick spin-coated PR films and RIE. The oxide film on the top side of the wafer receives the features that create a recess in the main body for the CNTs, while the silicon dioxide film on the bottom side of the wafer receives the features that decrease the thickness of the substrate where μfoam is etched. Next, the PR films are stripped off, and the top side of the wafer receives the features of the μfoam using contact photolithography on a 10-μm-thick spin-coated PR film. After that, the bottom of the wafer is etched 250 μm using DRIE. The wafer is then mounted on a quartz handler wafer using PR, leaving the top side of the wafer readily accessible for processing. Next, the features of the μfoam are etched 220 μm deep using DRIE. The PR on the top side of the wafer is stripped off using an oxygen plasma, and a 30-μm deep etch is carried out both to complete the μfoam

and to create a recess for the CNTs. Finally, the silicon wafer is detached from the quartz wafer using acetone.

B. Top Wafer Process Flow

The silicon dioxide films on both sides of the wafer are etched using contact photolithography on 10-μm-thick spin-coated PR films and RIE. The oxide film on the top side of the wafer receives the features of the extractor gate (extractor grid and extractor boundary) and the assembly springs, while the silicon dioxide film on the bottom side of the wafer receives the features that decrease the thickness of the extractor gate where the grid is etched. Next, the PR films are stripped off. After that, the bottom of the wafer is etched 400 μm using DRIE. The wafer is then mounted on a quartz handler wafer using PR, leaving the top side of the wafer readily accessible for processing. Next, the features of the extractor grid, extractor boundary, and assembly springs are etched through the wafer. Once the extractor grid is fully etched, the region is protected with Kapton tape until the rest of the etch is completed. At the end of the DRIE step, the extractors are detached from the silicon substrate. Finally, the silicon wafer is detached from the quartz wafer using acetone, and the extractors are collected.

C. Final Processing

After the processing described in Section III-A and B, the wafers and the extractor gates are cleaned using a piranha bath, and then, they are dipped in 49% pure HF for 5 min to strip the silicon dioxide films. Next, the wafers and the extractor grids are RCA cleaned. The wafers are aligned and brought in contact for 12 hr while being pressed with 10 kN of force, and then, the wafer stack is annealed at 1050 °C in nitrogen for 1 hr. A 1-μm-thick thermal oxide film is grown on both the wafer stack and the extractor gates to smooth the DRIE-created surfaces. After that, the main bodies of the ionizers are die-sawed from the wafer stack using contact photolithography on a 10-μm-thick spin-coated PR, RIE of the silicon dioxide film, and DRIE of the silicon substrate. The extractor gates and main bodies of the ionizers are dipped in a 49% pure HF bath to strip the oxide film. Next, a 5-μm-thick PECVD silicon dioxide film is deposited on the boundary of the extractor gates using a shadow mask to avoid coating the extractor grid. After all this processing is completed, the extractor gate is assembled to the main body of the ionizer, and a 7-nm-thick e-beam evaporated Ni film is deposited on the μfoam using the extractor gate as a shadow mask. The extractor gate is then disassembled, and sparse forests of PECVD CNTs are grown on the μfoam using the PECVD CNT growth process described by Teo *et al.* [60]. The CNTs are about 25 μm long. Finally, the extractor gate is re-assembled to the main body.

IV. Experimental Characterization

Devices fabricated as described in Section III were tested as electron field emitters in high vacuum (10^{-8} torr) and as EIIs using argon at pressures between 5×10^{-7} and 2.1×10^{-2} torr. Analysis of the data demonstrates that the electron currents are field emitted by the CNTs and that the ionization data follow the electron impact ionization model. Ion currents that are as large as 139 μA, with 19% ionization efficiency, were measured.

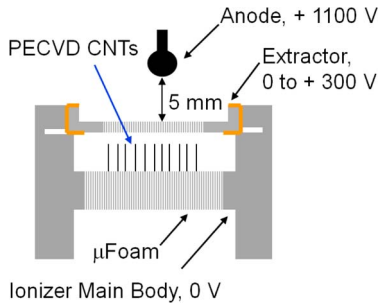

Fig. 6. Schematic of the field-emission testing setup.

A. Field-Emission Tests

Experimental Setup: Fig. 6 shows a schematic of the testing setup that is used to characterize the devices as electron sources. The test setup used a set of Keithley 237s controlled by Labview to bias voltages to the main body of the device, the extractor grid, and a suspended electrode, i.e., collector. This instrumentation is able to measure a maximum current of 10 mA and to apply a bias voltage between -1100 and $+1100$ V. When the main body of the device is biased at a negative voltage with respect to the extractor gate, electrons are field emitted from the CNTs on the main body, and a fraction of them is transmitted through the extractor gate. The collector is a 2-mm-diameter metallic sphere suspended about 5 mm above the extractor. The collector was biased at $+1100$ V during the field-emission tests. The collector allows us to discriminate between leakage current through the dielectric and electron emission, and it also let us estimate the electron current transmission of the extractor gate. If there is a linear dependence between the current intercepted by the extractor and the current collected by the suspended electrode, it can be concluded that both currents have the same physical origin. Since the collector has no direct electrical connection to the main body of the device, the origin of the measured currents cannot be the leakage current through the silicon dioxide that separates the extractor gate and the main body. We also conducted reverse-polarity tests to verify that the measured currents were field emitted, and we verified that the current emitted by the main body was equal to the grid current plus the collector current. In addition, we conducted FN analysis of the data to verify that the measured currents were field emitted by the CNT forests.

Field-Emission IV Characteristics: Depending on the doping concentration of the wafers used to fabricate the device, the device can emit anywhere between microampere-level [53] and milliampere-level electron currents [52] for bias voltages between 100 and 450 V. In particular, Fig. 7 shows the IV characteristics of a device made of silicon wafers with a resistivity of 5 $\Omega \cdot$ cm. This device has a start-up voltage of about 150 V (emission current above 10^{-10} A), and it emits about 68 μA of electron current when biased at 348 V. Fig. 8 shows a plot of the current transmitted by the extractor gate versus the current intercepted by the extractor gate data shown in

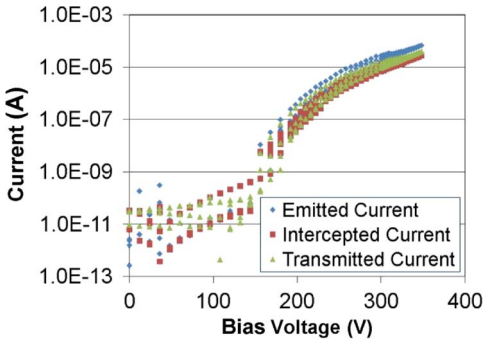

Fig. 7. Current emitted by the main body, current intercepted by the extractor, and current transmitted by the extractor for a MEMS/NEMS CNT ionizer made of 5-Ω · cm silicon wafers.

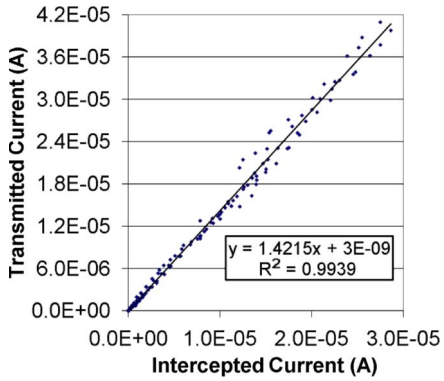

Fig. 8. Current transmitted by the extractor gate versus current intercepted by the extractor gate for the device with the data shown in Fig. 7.

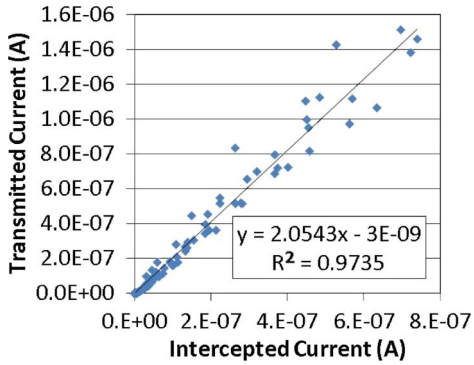

Fig. 9. Current transmitted by the extractor gate current versus current intercepted by the extractor gate for a CNT ionizer made with silicon substrates with a resistivity of 5 Ω · cm. The transmission through the extractor is better than 66%.

Fig. 7. Fig. 8 clearly shows that there is a linear dependence between the two currents (correlation $R^2 > 0.99$), suggesting that the currents measured in the experiment are field emitted. Based on Fig. 8, we estimate a 59% transmission through the extractor gate of the electron current emitted by the main body. This value is more than an order of magnitude larger than the transmission of an unaligned extraction gate using a similar emitting substrate [52]. We have tested devices with as much as 66% electron current transmission through the gate while emitting less current, as shown in Fig. 9.

FN Analysis: An analysis of the IV characteristics of the device would help us further corroborate that the measured

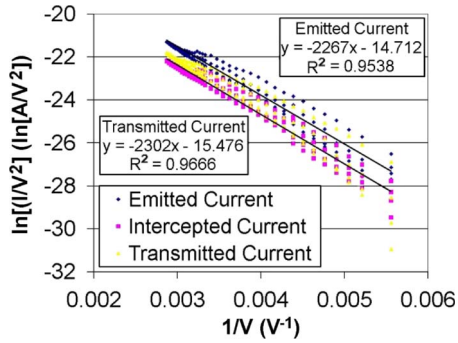

Fig. 10. FN plot of the data shown in Fig. 7. The transmitted, intercepted, and emitted current data describe the parallel straight lines in the FN plot.

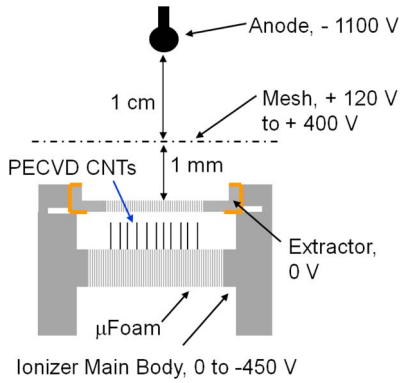

Fig. 11. Schematic of the electron impact ionization testing setup.

currents were field emitted by the CNT forests. Fig. 10 shows the FN plot ($\ln[I/V_G^2]$ versus V_G^{-1}) of the data shown in Fig. 7. The data in the FN plot describe parallel straight lines that evidence good correlation with the FN model ($R^2 > 0.95$). An average field factor β of 3×10^5 cm^{-1} is estimated from the slope of the FN plot, assuming that the workfunction for graphite is 4.8 eV. As a conservative estimate, $\beta \sim r^{-1}$ [47]. Therefore, a CNT tip radius of 33.3 nm is estimated from the FN plot, which is in good agreement with the 36-nm tip radius estimate from SEMs [see Fig. 2(e)].

B. Electron Impact Ionization Tests

Experimental Setup: Fig. 11 shows a schematic of the testing setup used to characterize the devices as EIIs, with argon at pressures between 5×10^{-7} and 2.2×10^{-2} torr. We measured the pressure with a Bayard–Alpert gauge from Varian, Inc. (Lexington, MA), which was directly connected to the vacuum chamber, and it is able to measure between 5×10^{-10} and 3×10^{-2} torr. The electron impact ionization testing setup is very similar to the field-emission testing setup shown in Fig. 6, although the electron impact ionization setup includes a fourth electrode. In the electron impact ionization tests, the main body of the device is still biased negatively with respect to the extractor gate to field emit electrons (the extractor was biased at 0 V, while the main body was biased at a voltage between 0 and -530 V). The fourth electrode is a high-transparency mesh that is biased at a positive voltage with respect to the extractor gate. The mesh attracts the electrons that are transmitted by the extractor gate to make them ionize the surrounding neutral

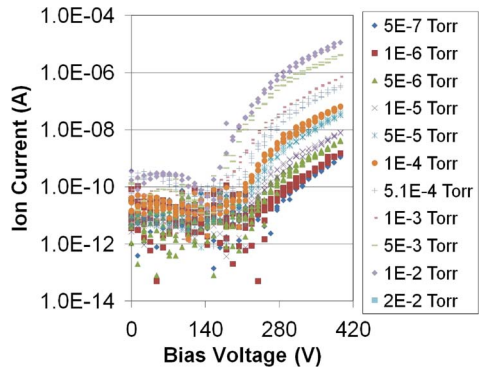

Fig. 12. Ion current versus emitter-to-extractor bias voltage or the ionizer with the field-emission data shown in Fig. 7.

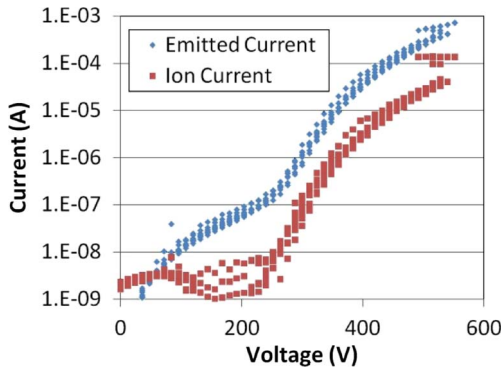

Fig. 13. Ion current versus emitter-to-extractor bias voltage of an ionizer made from silicon wafers with 5-Ω · cm resistivity. The data were taken with argon at a pressure of 21 mtorr.

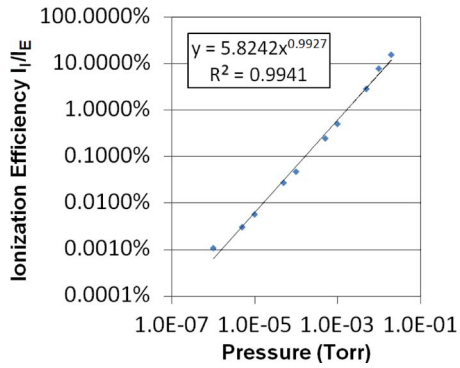

Fig. 14. Ion-current-to-electron-current ratio versus pressure of the data shown in Fig. 12.

gas molecules by collision. The suspended collector electrode is biased at a negative voltage to attract the ions that are formed in the ionization region. The collector was usually biased at -1100 V during the electron impact ionization tests, but we did not see any appreciable difference in the data as long as the collector voltage was negative. We typically biased the mesh electrode at $+400$ V with respect to the extractor electrode, but we did not see a substantial variation in the data when we varied the mesh electrode voltage down to $+120$ V. Our experimental setup does not do a good job of defining a constant-potential region where the ionization takes place (ideally, the mesh electrode should be a high-transparency cage), which would allow us to choose a potential that maximizes the total electron impact ionization cross section. Instead, the space between the mesh and the collector electrodes has a nonzero electric field that locally varies the electric potential, which defines the local total electron impact ionization cross section.

IV Characteristics: Fig. 12 shows the electron impact ionization data of the device with the field-emission data shown in Fig. 7. In the data, the pressure was varied between 5×10^{-7} and 2×10^{-2} torr, and the bias voltage between the main body and the extractor was varied between 0 and 396 V. From Fig. 12, it can be seen that the constant-pressure IV characteristics are parallel curves, as expected from the linear dependence of the ion current on the gas pressure for a fixed electron current shown in (1). In this data set, the device operated at a maximum pressure of 20 mtorr, and it produced up to 22.5 μA of ion current while emitting 140 μA of electron current (55-mW power consumption and an ion-to-electron current ratio of 0.16). We also tested devices that produced larger ion currents. For example, Fig. 13 shows the ion and electron current versus the extractor bias voltage data at 21 mtorr from a device in the same batch as the device previously discussed. The data were collected while conducting a series of six extractor voltage sweeps. The ionizer produced a maximum ion current of 0.139 mA while emitting 0.738 mA of electron current during the last voltage sweep of the series (0.39-W power consumption and an ion-to-electron current ratio of 0.19). It is clear from Fig. 13 that there was a sudden change in the IV characteristics of the device in the last sweep, i.e., more ion and electron currents for the same extractor bias voltage. The change in the IV characteristics was not permanent because we were able to duplicate the data shown in Fig. 13 whenever we conducted a series of multiple sweeps of the extractor bias voltage after letting the ionizer be inactive for a few minutes. Therefore, the experimental behavior of the IV characteristics suggests some kind of hysteresis. We speculate that the reversible increase in the field factor of the ionizer is due to an effect that is analogous to the well-known pull-in effect in surface micromachined MEMS [18]. The increase in the field factor could have been caused by the reduction of the separation between the CNT tips and the extractor due to buckling of the extractor grid, which could have been caused by the thermal expansion of the grid due to the electron current that it intercepted (a peak power of about 0.16 W was dissipated by the extractor gate) and of the electrostatic suction of the extractor gate toward the main body due to the bias voltage.

C. Discussion

Equation (1) can be seen as an ionization efficiency, i.e., as the ratio of the number of ions formed to the number of electrons used in the ionization process [61]. Fig. 14 shows a plot of the ion-current-to-electron-current ratio at 396 V versus the pressure of the data shown in Fig. 12. A fit of the data shown in Fig. 14 suggests that the data follow the electron impact ionization model because the current ratio is proportional to the pressure to the 0.993 power, the correlation R^2 of the fit is better than 0.99, and the 5.82 coefficient of the fit implies an average total ionization cross section of 1.95×10^{-16} cm^{-2}, which is within the range of total ionization cross sections for the range

of voltage that are present in the ionization region [62]. The data shown in Fig. 12 have a maximum ionization efficiency of 16%, while the data shown in Fig. 13 have an ionization efficiency of 19%, which is several orders of magnitude higher than the ionization efficiency that is typically attained by thermionic EIIs [13]. Looking at (1), it is possible to implement field-emission-based and thermionic-emission-based ion sources with the same (and optimal) ionization efficiency at a given pressure if the effective ionization length is the same and the effective ionization cross section is maximum. The key advantage of the CNT-based EII that we report over the thermionic-based EIIs is its capability to operate at orders of magnitude higher pressure than the thermionic-based EIIs without degradation, which leads to the capability to achieve orders of magnitude of higher ionization efficiency, in combination with the resistance to oxygen that CNT-based cold cathodes has, as other researchers have shown [51]. If one uses a differential pumping scheme where the thermionic electron source is held at high vacuum but the ionization region is held at a higher pressure, then it is arguable that the thermionic-based EIIs would perform just as well as the CNT-based EIIs. However, this architecture clearly introduces more complexity to the portable MS design, and it would visibly increase the energy required for pumping.

While conducting the electron impact ionization tests, we tried multiple times to collect data at pressures higher than 21 mtorr, but instead, the pressure increase always led to the creation of a plasma within the vacuum chamber triggered by the high voltage biased to the spherical electrode. However, as we had previously reported [52], the devices did not suffer any noticeable loss of performance after striking a plasma. Nonetheless, it is possible to burn out some of the CNTs and, hence, shift the IV characteristics of the device if the bias voltage between the extractor gate and the emitters is large enough. Fortunately, we showed in a previous report that it is possible to limit the emitted electron current [53], which should reduce the likelihood of field emitter burn-out.

Our ionizer compares favorably to other MEMS/NEMS-enabled ionizers reported in the literature. For example, the electron current of our devices is several orders of magnitude larger than what was reported by Liu *et al.*, with nanostructured boron nitride cathodes, and their operational voltage is visibly higher [63]. Also, the electron current that our CNT-based ionizer attained is several orders of magnitude larger than the electron current achieved by the MEMS thermionic ionizers developed by Yoon *et al.* (7 nA using a tungsten filament [33] and 280 nA using a nickel filament [34]) or several orders of magnitude larger than the electron current from the CNT-based cold cathodes reported by Yoon *et al.* (18.5 μA at 175 V [34]) or Hwang *et al.* (80 μA at 1.1 kV [35]). Moreover, the ionization efficiency of our devices is almost four times larger than the ionization efficiency reported by Chen *et al.* using arrays of double-gated isolated PECVD CNTs, with argon at 5.6 mtorr [48]. In addition, our devices have an estimated field factor from the FN plot that is 50% larger than the corresponding values reported by Manohara *et al.* [39], which implies that our ionizer can extract more current and, hence, produce more ion current with less bias voltage. We speculate that the smaller field factor in the work of Manohara *et al.* is related to the shadowing effect that their CNTs suffer due to their proximity within the same fiber. Finally, Bower *et al.* reported a very interesting CNT-based EII with 30-μm CNT tips-to-extractor separation and 280-μm extractor-to-collector separation (i.e., ionization length) [36]. They reported operation of their EII at pressures as high as 0.1 torr. Using Ar, Bower *et al.* reported an ionization efficiency of 0.009 at 20 mtorr and 0.05 at 0.1 torr. Our ionization efficiency at 20 mtorr with the same gas is more than 20 times larger. We believe that the ionization efficiency of their EII is visibly smaller than the ionization efficiency of our EII at the same pressure and with the same gas, because their EII has a very short ionization length. Based on their data, we estimate that their EII would have a similar ionization efficiency if its ionization length would be as large as ours.

V. Conclusion

We reported the fabrication and experimental characterization of a PECVD CNT-based MEMS/NEMS electron impact gas ionizer with an integrated extractor gate for portable MS. The extractor gate is integrated to the ionizer using a set of DRIE springs that are capable of extractor gate re-assembly with micrometer-scale precision. The devices were tested as field emitters in high vacuum $(10^{-8}$ torr) and as EIIs using argon at pressures of up to 21 mtorr. The ionization data follow the electron impact ionization model. The extractor gate transmits up to 66% of the emitted electron current, and the devices produced up to 0.139 mA of ion current, with 19% ionization efficiency, while consuming 0.39 W.

References

[1] D. H. Holkeboer, T. L. Karandy, F. C. Currier, L. C. Frees, and R. E. Ellefson, "Miniature quadrupole residual gas analyzer for process monitoring at millitorr pressures," *J. Vac. Sci. Technol. A, Vac. Surf. Films*, vol. 16, no. 3, pp. 1157–1162, May 1998.

[2] R. T. Short, D. P. Fries, M. L. Kerr, and R. H. Byrne, "Field chemical analysis using real-time in-water mass spectrometry," in *Proc. IEEE Conf. Exhib. Oceans*, Sep. 2000, vol. 1, pp. 605–609.

[3] A. Chutjian, M. R. Darrach, V. Garkanian, S. P. Jackson, T. D. Molsberry, O. Orient, D. Karmon, P. M. Holland, and D. Aalami, "A miniature quadrupole mass spectrometer array and GC for space flight: Astronaut EVA and cabin-air monitoring," presented at the SAE International Symposium on Environmental Sensors, Toulouse, France, Jul. 10–14, 2000.

[4] R. R. Reston and E. S. Kolesar, "Silicon-micromachined gas chromatography system used to separate and detect ammonia and nitrogen dioxide—Part I: Design, fabrication, and integration of the gas chromatography system," *J. Microelectromech. Syst.*, vol. 3, no. 4, pp. 134–146, Dec. 1994.

[5] R. R. Reston and E. S. Kolesar, "Miniature gas chromatography system realized using conventional VLSI fabrication techniques applied to quantifying toxic environmental pollutants," in *Proc. IEEE NAECON*, May 1994, vol. 1, pp. 327–333.

[6] O. J. Orient, A. Chutjian, and V. Garkanian, "Miniature, high-resolution, quadrupole mass-spectrometer array," *Rev. Sci. Instrum.*, vol. 68, no. 3, pp. 1393–1397, Mar. 1997.

[7] B. Ghodsian, M. Parameswaran, and M. Syrzycki, "Gas detector with low cost micromachined field ionization tips," *IEEE Electron Device Lett.*, vol. 19, no. 7, pp. 241–243, Jul. 1998.

[8] N. Sillon and R. Baptist, "Micromachined mass spectrometer," *Sens. Actuators B, Chem.*, vol. 83, no. 1–3, pp. 129–137, Mar. 2002.

[9] D. Wiberg, N. V. Myung, B. Eyre, K. Shcheglov, O. Orient, E. Moore, and P. Munz, "LIGA fabricated two-dimensional quadrupole array and scroll pump for miniature gas chromatograph/mass spectrometer," *Proc. SPIE*, vol. 4878, pp. 8–13, 2003.

[10] W. C. Wang, "Micromechanical devices at JPL for space exploration," in *Proc. IEEE Aerosp. Conf.*, 1998, vol. 1, pp. 461–470.

[11] P. M. Holland, A. Chutjian, M. R. Darrach, O. J. Orient, and D. Karmon, "Miniaturized GCMS instrumentation for in situ measurements: Micro gas chromatography coupled with miniature quadrupole array and Paul ion trap mass spectrometers," *Proc. SPIE*, vol. 4878, pp. 1–7, 2003.

[12] R. J. Ferran and S. Boumsellek, "High-pressure effects in miniature arrays of quadrupole analyzers for residual gas analysis from 10^{-9} to 10^{-2} torr," *J. Vac. Sci. Technol. A, Vac. Surf. Films*, vol. 14, no. 3, pp. 1258–1265, May 1996.

[13] J. H. Gross, *Mass Spectrometry: A Textbook*. Berlin, Germany: Springer-Verlag, 2006.

[14] S. Boumsellek and R. J. Ferran, "Trade-offs in miniature quadrupole designs," *J. Amer. Soc. Mass Spectrom.*, vol. 12, no. 6, pp. 633–640, Jun. 2001.

[15] E. R. Badman and R. G. Cooks, "Special feature: Perspective, miniature mass analyzers," *J. Mass Spectrom.*, vol. 35, pp. 659–671, 2000.

[16] C. Janfelt, N. Talaty, C. C. Mulligan, A. Keil, Z. Ouyang, and R. G. Cooks, "Mass spectra of proteins and other biomolecules recorded using a handheld instrument," *Int. J. Mass Spectrom.*, vol. 278, no. 2/3, pp. 166–169, Dec. 2008.

[17] M. Yang, T.-Y. Kim, H.-C. Hwang, S.-K. Yi, and D.-H. Kim, "Development of a palm portable mass spectrometer," *J. Amer. Soc. Mass Spectrom.*, vol. 19, no. 10, pp. 1442–1448, Oct. 2008.

[18] S. D. Senturia, *Microsystem Design*. Berlin, Germany: Springer-Verlag, 2004.

[19] S. C. Terry, J. H. Jerman, and J. B. Angell, "A gas chromatographic air analyzer fabricated on a silicon wafer," *IEEE Trans. Electron Devices*, vol. ED-26, no. 12, pp. 1880–1886, Dec. 1979.

[20] E. Wapelhorst, J.-P. Hauschild, and J. Müller, "Complex MEMS: A fully integrated TOF micro mass spectrometer," *Sens. Actuators A, Phys.*, vol. 138, no. 1, pp. 22–27, Jul. 2007.

[21] S. Pau, C. S. Pai, Y. L. Low, J. Moxom, P. T. A. Reilly, W. B. Whitten, and J. M. Ramsey, "Microfabricated quadrupole ion trap for mass spectrometer applications," *Phys. Rev. Lett.*, vol. 96, no. 12, pp. 120801-1–120801-4, Mar. 2006.

[22] A. B. Kanu, P. Dwivedi, M. Tam, L. Matz, and H. H. Hill, Jr., "Ion mobility-mass spectrometry," *J. Mass Spectrom.*, vol. 43, no. 1, pp. 1–22, Jan. 2008.

[23] S. Taylor, J. J. Tunstall, R. R. A. Syms, T. J. Tate, and M. M. Ahmad, "Initial results for a quadrupole mass spectrometer with a silicon micromachined mass filter," *Electron. Lett.*, vol. 34, no. 6, pp. 546–547, Mar. 1998.

[24] R. Syms, T. J. Tate, M. M. Ahmad, and S. Taylor, "Design of a microengineered electrostatic quadrupole lens," *IEEE Trans. Electron Devices*, vol. 45, no. 11, pp. 2304–2311, Nov. 1998.

[25] S. Taylor, J. J. Tunstall, J. H. Leck, R. Tindall, P. Julian, J. Batey, R. R. A. Syms, T. J. Tate, and M. M. Ahmad, "Performance improvements for a miniature quadrupole with a micromachined mass filter," *Vacuum*, vol. 53, no. 1/2, pp. 203–206, May 1999.

[26] M. Geear, R. R. A. Syms, S. Wright, and A. S. Holmes, "Monolithic MEMS quadrupole mass spectrometers by deep silicon etching," *J. Microelectromech. Syst.*, vol. 14, no. 5, pp. 1156–1166, Oct. 2005.

[27] L. F. Velásquez-García, K. Cheung, and A. I. Akinwande, "An application of 3D MEMS packaging: Out-of-plane quadrupole mass filters," *J. Microelectromech. Syst.*, vol. 16, no. 6, pp. 1430–1438, 2008.

[28] P. S. Riehl, K. L. Scott, R. S. Muller, R. T. Howe, and J. A. Yasaitis, "Electrostatic charge and field sensors based on micromechanical resonators," *J. Microelectromech. Syst.*, vol. 12, no. 5, pp. 577–589, Oct. 2003.

[29] Y. Zhu, J. Lee, and A. Seshia, "System-level simulation of a micromachined electrometer using a time-domain variable capacitor circuit model," *J. Micromech. Microeng.*, vol. 17, no. 5, pp. 1059–1065, May 2007.

[30] S. E. Vargo, E. P. Muntz, G. R. Shiflett, and W. C. Tang, "The Knudsen compressor as a micro and macroscale vacuum pump without moving parts or fluids," *J. Vac. Sci. Technol. A, Vac. Surf. Films*, vol. 17, no. 4, pp. 2308–2313, Jul. 1999.

[31] S. McNamara and Y. B. Gianchandani, "On-chip vacuum generated by a micromachined Knudsen pump," *J. Microelectromech. Syst.*, vol. 14, no. 4, pp. 741–746, Aug. 2005.

[32] S. Wright and Y. B. Gianchandani, "Contaminant gas removal using thin-film Ti electrode microdischarges," *Appl. Phys. Lett.*, vol. 95, no. 11, pp. 11504-1–11504-3, Sep. 2009.

[33] H. J. Yoon, J. H. Kim, T. G. Park, S. S. Yang, and K. W. Jung, "The test of hot electron emission for the micro mass spectrometer," *Proc. SPIE*, vol. 4408, pp. 360–367, 2001.

[34] H. J. Yoon, S. H. Song, N. T. Hong, K. W. Jung, S. Lee, and S. S. Yang, "Fabrication of two types of micro ion sources for a micro time-of-flight mass spectrometer," *J. Micromech. Microeng.*, vol. 17, no. 8, pp. 1542–1548, 2007.

[35] J. S. Hwang, S. W. Park, J. B. Cho, K. S. Oh, S. S. Yang, S. Lee, K. H. Koh, and K. W. Jung, "The micro mass spectrometer with a carbon nano structure ion source," in *Proc. 1st IEEE Int. Conf. Nano/Micro Eng. Molecular Syst.*, Zhuhai, China, 2006, pp. 1220–1223.

[36] C. A. Bower, K. H. Gilchrist, J. R. Piascik, B. R. Stoner, S. Natarajan, C. B. Parker, S. D. Wolter, and J. T. Glass, "On-chip electron-impact ion source using carbon nanotube field emitters," *Appl. Phys. Lett.*, vol. 90, p. 124 102, Mar. 2007.

[37] L.-Y. Chen, L. F. Velasquez-Garcia, X. Wang, K. Teo, and A. I. Akinwande, "A micro ionizer for portable mass spectrometers using double-gated isolated vertically aligned carbon nanofiber arrays," in *IEDM Tech. Dig.*, Washington, DC, Dec. 2007, pp. 843–846.

[38] S.-J. Park, J. G. Eden, and K.-H. Park, "Carbon nanotube-enhanced performance of microplasma devices," *Appl. Phys. Lett.*, vol. 84, no. 22, pp. 4481–4483, May 2004.

[39] H. M. Manohara, M. J. Bronikowski, R. Toda, E. Urgiles, R. H. Lin, K. Y. Yee, A. B. Kaul, and J. Hong, "Application specific electrode-integrated nanotube cathodes (ASINCs) for miniature analytical instruments for space exploration," *Proc. SPIE*, vol. 6959, p. 695 906, 2008, DOI:10.1117/12.777322.

[40] L. Gao, Q. Song, R. J. Noll, J. Duncan, R. G. Cooks, and Z. Ouyang, "Glow discharge electron impact ionization source for miniature mass spectrometers," *J. Mass Spectrom.*, vol. 42, no. 5, pp. 675–680, May 2007.

[41] R. G. Longwitz, H. van Lintel, and P. Renaud, "Study of micro-glow discharges as ion sources for ion mobility spectrometry," *J. Vac. Sci. Technol. B, Microelectron. Process. Phenom.*, vol. 21, no. 4, pp. 1570–1573, Jul. 2003.

[42] J. C. T. Eijkel, H. Stoeri, and A. Manz, "A molecular emission detector on a chip employing a direct current microplasma," *Anal. Chem.*, vol. 71, no. 14, pp. 2600–2606, Jun. 1999.

[43] L. J. Kieffer and G. H. Dunn, "Electron impact ionization cross-section data for atoms, atomic ions, and diatomic molecules: I. Experimental data," *Rev. Mod. Phys.*, vol. 38, no. 1, pp. 1–35, Jan. 1966.

[44] S. Dushman, "Thermionic emission," *Rev. Mod. Phys.*, vol. 2, no. 4, pp. 381–476, 1930.

[45] E. de Hoffmann and V. Stroobant, *Mass Spectrometry: Principles and Applications*. West Sussex, U.K.: Wiley, 2002.

[46] R. Gomer, *Field Emission and Field Ionization*. New York: AIP, 1961.

[47] D. G. Pflug, "Modeling the effects of device scaling on field emitter array performance," M.S. thesis, MIT, Cambridge, MA, 1996.

[48] L. Dvorson, G. Sha, I. Kymissis, C.-Y. Hong, and A. I. Akinwande, "Electrical and optical characterization of field emitter tips with integrated vertically stacked focus," *IEEE Trans. Electron Devices*, vol. 50, no. 12, pp. 2548–2558, Dec. 2003.

[49] C. M. Marrese and J. E. Polk, "Molybdenum field emission array cathode performance in primarily xenon environments: Preliminary experimental results at low operating voltages," presented at the 36th AIAA/ASME/SAE/ASEE Joint Propulsion Conf. and Exhibit, Huntsville, AL, Jul. 16–19, 2000, Paper AIAA-2000-3266.

[50] M. S. Dresselhaus, G. Dresselhaus, and P. Avouris, Eds., *Carbon Nanotubes: Synthesis, Structure, Properties, and Applications*. Berlin, Germany: Springer-Verlag, 2001.

[51] C. J. Gasdaska, P. Falkos, V. Hruby, M. Robin, N. Demmons, R. McCormick, D. Spence, and J. Young, "Testing of carbon nanotube field emission cathodes," presented at the 40th AIAA/ASME/SAE/ASEE Joint Propulsion Conf. and Exhibit, Fort Lauderdale, FL, Jul. 11–14, 2004, Paper AIAA 2004-3427.

[52] L. F. Velásquez-García and A. I. Akinwande, "A PECVD CNT-based open architecture field ionizer for portable mass spectrometry," in *Proc. 21st IEEE Int. Conf. Micro Electro Mech. Syst.*, Tucson, AZ, Jan. 2008, pp. 742–745.

[53] L. F. Velásquez-García, B. Gassend, and A. I. Akinwande, "CNT-based gas ionizers with integrated MEMS gate for portable mass spectrometry applications," in *Proc. 15th Int. Conf. Solid-State Sensors, Actuators Microsyst.*, Denver, CO, Jun. 21–25, 2009, pp. 1646–1649.

[54] W. I. Milne, K. B. K. Teo, G. A. J. Amaratunga, P. Legagneux, L. Gangloff, J.-P. Schnell, V. Semet, V. T. Binh, and O. Goening, "Carbon nanotubes as field emission sources," *J. Mater. Chem.*, vol. 14, no. 6, pp. 933–943, 2004.

[55] L. F. Velásquez-García, A. I. Akinwnade, and M. Martinez-Sanchez, "Precision hand assembly of MEMS subsystems using DRIE patterned deflection spring structures: An example of an out-of-plane substrate assembly," *J. Microelectromech. Syst.*, vol. 16, no. 3, pp. 598–612, Jun. 2007.

[56] B. Gassend, L. F. Velásquez-García, and A. I. Akinwande, "Precision in-plane hand assembly of bulk-microfabricated components for high voltage MEMS arrays applications," *J. Microelectromech. Syst.*, vol. 18, no. 2, pp. 332–346, 2009.
[57] H. Takemura, Y. Tomihari, N. Furutake, F. Matsuno, M. Yoshiki, N. Takada, A. Okamoto, and S. Miyano, "A novel vertical current limiter fabricated with a deep trench forming technology for highly reliable field emitter arrays," in *IEDM Tech. Dig.*, Washington, DC, Dec. 1997, pp. 709–712.
[58] L. F. Velásquez-García, B. Adeoti, Y. Niu, and A. I. Akinwande, "Uniform high current field emission of electrons from Si and CNF FEAs individually controlled by Si pillar ungated FETs," in *IEDM Tech. Dig.*, Washington, DC, Dec. 2007, pp. 599–602.
[59] P. H. Thompson, *Compressible-Fluid Dynamics,* 3rd ed. New York: McGraw-Hill, 1988.
[60] K. B. K. Teo, S.-B. Lee, M. Chhowalla, V. Semet, V. T. Binh, O. Groening, M. Castignolles, A. Loiseau, G. Pirio, P. Legagneux, D. Pribat, D. G. Hasko, H. Ahmed, G. A. J. Amaratunga, and W. I. Milne, "Plasma enhanced chemical vapour deposition carbon nanotubes/nanofibers—How uniform do they grow?" *Nanotechnology*, vol. 14, pp. 204–211, 2003.
[61] A. D. McNaught and A. Wilkinson, Eds., *IUPAC Compendium of Chemical Terminology,* 2nd ed. Oxford, U.K.: Blackwell, 1997.
[62] H. C. Straub, P. Renault, B. G. Lindsay, K. A. Smith, and R. F. Stebbings, "Absolute partial and total cross sections for electron-impact ionization of argon from threshold to 1000 eV," *Phys. Rev. A, Gen. Phys.*, vol. 52, no. 2, pp. 1115–1124, Aug. 1995.
[63] T. Liu, D. Morris, J. Zagel, C. Cionca, Y. Li, C. Smith, A. Riposan, A. Gallimore, B. Gilchrist, and R. Clarke, "Use of boron nitride for field effect electron emission," presented at the 43rd AIAA/ASME/SAE/ASEE Joint Propulsion Conf. and Exhibit, Cincinnati, OH, Jul. 8–11, 2007, Paper AIAA-2007-5253.

Luis Fernando Velásquez-García (M'09) received the Mechanical Engineer degree (*magna cum laude* and valedictorian of the School of Engineering) and the Civil Engineer degree (*magna cum laude* and valedictorian of the School of Engineering) from the Universidad de Los Andes, Bogotá, Colombia, in 1998 and 1999, respectively, and the M.S. and Ph.D. degrees from the Department of Aeronautics and Astronautics, Massachusetts Institute of Technology (MIT), Cambridge, in 2001 and 2004, respectively.

In 2004, after completing his studies, he became a Postdoctoral Associate in the Microsystems Technology Laboratories (MTL), MIT, where he was appointed as a Research Scientist in 2005. Since 2009, he has been a Principal Scientist and Core Member with MTL. He is an expert in micro- and nanofabrication technologies, and his research focuses on the application of micro- and nanotechnology to multiplexed scaled-down systems to attain better performance. He has conducted research in micro- and nanotechnologies applied to electrospray, carbon-nanotube-based devices, 3-D packaging, mass spectrometry, propulsion, and chemical reactors. He has authored more than 15 journal publications and 30 conference proceedings entries. He is the holder of six patents on MEMS technologies.

Dr. Velásquez-García is a full member of Sigma Xi and a Senior Member of the American Institute of Aeronautics and Astronautics (AIAA).

Blaise Laurent Patrick Gassend was born in Nice, France, in 1978. He received the Dipl. Ing. degree from the Ecole Polytechnique, Palaiseau, France, in 2001, and the M.S. degree in physical random functions and the Ph.D. degree in microfabricated electrospray thruster arrays from the Department of Electrical Engineering and Computer Science, Massachusetts Institute of Technology, Cambridge, in 2003 and 2007, respectively.

After graduating, he was with Exponent, Inc., Menlo Park, CA, as an Associate in the Electrical and Semiconductor Practice, where he consulted on failure analysis and litigation support. Since 2009, he has been the Hardware Interface Guru at Willow Garage, Inc., Menlo Park, working on hardware and software for the PR2 robot.

Akintunde Ibitayo (Tayo) Akinwande (S'81–M'86–SM'04–F'08) received the B.Sc. degree in electrical and electronic engineering from the University of Ife, Ife, Nigeria, in 1978, and the M.S. and Ph.D. degrees in electrical engineering from Stanford University, Stanford, CA, in 1981 and 1986, respectively.

In 1986, he joined Honeywell International, Inc., Morristown, NJ, where he initially conducted research on GaAs complementary FET technology for very-high-speed and low-power signal processing. He later joined the Si Microstructures Group, where he conducted research on pressure sensors, accelerometers, and thin-film field emission and display devices. In January 1995, he joined the Microsystems Technology Laboratories, Massachusetts Institute of Technology (MIT), Cambridge, where his research focuses on microfabrication and electronic devices, with particular emphasis on smart sensors and actuators, intelligent displays, large-area electronics (macroelectronics), field-emission and field-ionization devices, mass spectrometry, and electric propulsion. He was a Visiting Professor in the Department of Engineering and an Overseas Fellow at Churchill College, Cambridge University, Cambridge, U.K., in 2002 and 2003. He is currently a Professor in the Department of Electrical Engineering and Computer Science, MIT. Since September 2009, he has been the Program Manager of the Microsystems Technology Office, Defense Advanced Research Projects Agency. He is the author of more than 100 journal publications and is the holder of numerous patents in the areas of MEMS, electronics on flexible substrates, and display technologies.

Prof. Akinwande was the recipient of a 1996 National Science Foundation CAREER Award. He is currently a member of the IEEE Nanotechnology Council. He has served on a number of Technical Program Committees for various conferences, including the Device Research Conference, the IEEE International Electron Devices Meeting, the IEEE International Solid-State Circuits Conference, the International Display Research Conference, and the International Vacuum Microelectronics Conference.